Science World Journal Vol. 20(No 4) 2025 https://dx.doi.org/10.4314/swj.v20i4.15
www.scienceworldjournal.org
ISSN: 1597-6343 (Online), ISSN: 2756-391X (Print)
Published by Faculty of Science, Kaduna State University

Full Length Research Article

DYNAMICS OF WILLIAMSON NANOFLUIDS OVER A STRETCHING SHEET WITH VARIABLE VISCOSITY, THERMAL CONDUCTIVITY, AND SORET-DUFOUR MECHANISM EFFECTS

*[1]Onwubuoya Cletus, [2]M.S. Dada, [3]Ogeh Kenneth Oke

[1]Department of Mathematics, Federal University of Medical and Health Sciences, Kwale, Delta State, Nigeria
[2]Department of Mathematics, University of Ilorin, Ilorin, Nigeria
[3]Department of Mathematical Sciences, Edwin Clark University, Kiagbodo, Delta State, Nigeria

*Corresponding Author Email Address: onwubuoyacletus@yahoo.com

ABSTRACT
This study investigates the two-dimensional, steady, incompressible flow of a Williamson nanofluid over a stretching sheet in the presence of a magnetic field, accounting for variable viscosity, thermal conductivity, and the Soret-Dufour effects. Williamson nanofluids, characterized by their non-Newtonian shear-thinning behavior, are widely used in industrial processes such as polymer extrusion, chemical engineering, and food processing. The coupling of magnetohydrodynamics (MHD) with variable thermophysical properties and cross-diffusion phenomena significantly influences heat and mass transfer performance, making it essential to explore these effects for practical applications. Numerical simulations are performed using the fourth-order Runge-Kutta method with the shooting technique to obtain velocity, temperature, and concentration profiles, along with skin friction, Nusselt, and Sherwood numbers. The study provides a comprehensive analysis of the impact of Williamson, magnetic, Soret, and Dufour parameters on flow and transport characteristics, offering valuable insights for optimizing engineering systems.

Keywords: Williamson nanofluid, Runge-Kutta method, Soret-Dufour, MHD, variable viscosity, thermal conductivity.

INTRODUCTION

The basic concept of MHD is the exploration of an electrically conducting fluid as a result of the imposition of a magnetic field. The production of a magnetic field is from an electric current. The applications of MHD are found in areas of engineering such as geophysics, metallurgy, and astrophysics. As a result of these applications, many scholars have explained the significance of MHD on fluid flow. Alhussain et al. (2021) examined magneto-bioconvective and thermal conductivity enhancement in nanofluid flow containing microorganisms. Their equations were changed from PDEs to ODEs using an appropriate similarity variables. The transformed ODEs were later solved by employing the numerical approach of Bvp4c code in MATLAB. It was found in their study that an increase in the magnetic parameter degenerates the energy field. Hassan et al. (2021) studied bioconvection transport of magnetized Walters-B nanofluid across a cylindrical disk with nonlinear radiative heat transfer. Their transformed equations were solved by implementing the bvp4c technique in MATLAB software. It was observed in their study that a larger magnetic parameter diminishes the velocity field. The study of Alzahrani and Khan (2021) discussed the significance of induced magnetic force bio-convective flow of radiative Maxwell nanofluid with activation energy. The shooting numerical technique was employed in solving their model equations. They observed that the reciprocal magnetic Prandtl number elevates the nanofluid temperature, concentration, and microorganisms profiles. The comparative study of magnetized flow of nanofluids between two parallel permeable stretching/shrinking surfaces was investigated by Nayak et al. (2021). The study of Hassan et al. (2022) studied thermal analysis of magnetized flow of AA7072-AA7075/blood-based hybrid nanofluids in a rotating channel. They employed the bvp4c solver in MATLAB software to solve their flow equations numerically. It was observed that a larger Reynolds number decreases the tangential velocity of blood-based hybrid nanofluids. Ali and Sandeep (2017) extensively discussed heat transfer of MHD with the radiative Cattaneo-Christov model. Their flow equations were solved numerically by employing the Runge-Kutta Felhberg integration scheme. They concluded that the applied transverse magnetic field resulted in uniform nanoparticle motion. Mutuku-Njane and Makinde (2013) considered the combined effect of buoyancy force alongside Navier slip on MHD flow of a nanofluid over a heated vertical porous plate. To solve their flow equations, the Fourth-order Runge-Kutta with the shooting technique was employed. They concluded in their study that the Hartmann number causes a decrease in the Nusselt number. Hayat et al. (2015) investigated the effect of an inclined magnetic field in the flow of third-grade fluid with variable thermal conductivity. Their resulting equations were solved using an appropriate solution. They concluded that the significance of the magnetic field parameter and inclination angle on the velocity possesses similar outcomes.

Numerical simulation of mixed convection squeezing hybrid nanofluid filled with magnetized ferroparticles was investigated by Nisar et al. (2020). They employed a similarity technique to change the governing PDEs to ODEs before implementing the Matlab bvp4c solver. They concluded that the squeezed number lessens the temperature field. Pallavi et al (2024) studied the effects of exponentially stretching sheet for MHD Williamson nanofluid with chemical reaction and thermal radiative. The governing non–linear partial differential equations were converted to a couple of nonlinear ordinary differential equations by using a similarity transformation, which were solved numerically using the Runge-Kutta-Fehlberg method along with the shooting technique. They reported that increasing the magnetic field parameter reduces the fluid velocity, while higher thermal radiation and Brownian motion parameters significantly enhance the heat transfer rate within the boundary region. El-Zahar et al. (2021) examined unsteady MHD

mixed convection flow of non-Newtonian Casson hybrid nanofluid within a stagnation zone. Their governing linear equations were solved numerically, and they observed that an increase in solid volume fraction and surface shear stresses enhances the rate of heat transfer. The study of Hussain et al. (2021) investigated the heat transport of a magneto-hydrodynamics hybrid nanofluid with thermal radiation influence. They solved the nonlinear differential equations of their model by implementing the bvp4c MATLAB algorithm. They suggested in the study that the nanofluid exploitation is very good in reducing production costs.

The mechanism of solute alongside thermal features in a Casson hybrid nanofluid based along side Ethylene Glycol has been investigated by Hafeez et al. (2021). They solved their flow equations numerically by utilizing the finite element approach with 10-8 tolerance. They concluded that the Soret-Dufour significantly influences the temperature and concentration field. Alzahrami et al. (2021) explored hybrid nanofluid flow through a penetrable medium with solar radiation. They solved their transformed equations by utilizing the HAM. They concluded in their study that a greater value of the Schmidt number decreases the concentration field. Kumar et al. (2018) elucidated the hydromagnetic unsteady slip stagnation flow of nanofluid together with suspension of mixed bio-convection. Their governing transport Buongiorno's model was converted to ODEs by utilizing the implicit finite difference scheme (IFDS). They concluded that the thermal slip gives a huge increase in skin friction coefficients. Waqas et al. (2021) examined the impact of MHD radiative flow of hybrid nanofluid over a rotating disk. They reduced the system of governing PDEs to ODEs by utilizing similarity transformations. They have now solved the transformed ODEs by utilizing the bvp4c in-built function in MATLAB. They concluded that the temperature field reduces due to a higher value of the Prandtl number. Chemical reaction on bio-convection nanofluid flow within double parallel plates in a rotating system by varying viscosity was examined by Tarakaramu and Narayana (2019). Their governing flow equations were solved numerically using the shooting method. They concluded that motile density distribution declines when thermal radiation and Brownian motion increase. The study of Akolade et al. (2021) examined the influence of thermophysical features on MHD squeezed flow on dissipative Casson fluid with radiative and chemical effects. They solved their governing equations of motion by utilizing the Chebyshev-based collocation approach. They concluded that their analysis finds application in polymer processing. Darcy-Forchheimer hybrid nanofluid flow over a stretching curved surface with mass alongside heat transfer was discussed by Saeed et al. (2021). Their governing coupled PDEs were changed to coupled ODEs by using an appropriate similarity transformation. They concluded that hybrid nanofluids serve as fast agents for heat transfer analysis when compared to common fluids. Onwubuoya and Dada (2021) investigated Soret, viscous dissipation, and thermal radiation effects on MHD free convective flow of Williamson liquid with variable viscosity and thermal conductivity. Their transformed governing equations were solved using SHAM. They reported that an increase in the Williamson parameter(β) leads to a decrease in the thickness of the hydrodynamic thermal layer. Ahmed et al (2020) examined the mechanism of both positive and negative effects of Soret–Dufour with heat and mass transfer processes over an accelerating permeable surface. The partial differential flow equations were simplified using similarity variables and were solved numerically using the spectral homotopy analysis method(SHAM). They reported that a positive Soret–Dufour enhances the boundary layer, whereas a negative Soret–Dufour parameter decreases the boundary layer. Zhang et al. (2021) studied the parametric study of hybrid nanofluid flow with heat transfer features past a fluctuating spinning disk. Their equations were solved numerically by utilizing the parametric continuation method. They concluded that water's thermophysical properties are boosted by close bonds existing between atoms of water (H++OH-) and silver ions Ag+. Mixed convective flow with analysis of heat transfer with MHD hybrid nanofluid over a stretching sheet was investigated by Ramzan et al. (2021). Their governing PDEs were changed to ODEs using an appropriate similarity transformation. The transformed ODEs were later solved by utilizing the HAM. They concluded that the hybrid nanofluid velocity increases for both slip and no-slip conditions. Arain et al. (2021) examined Reiner-Rivlin nanofluid flow within rotating circular plates with the squeezing phenomenal induced magnetic impact and activation energy. A semi-numerical technique called the differential transform method was used to solve their equations. They draw a conclusion that nanoparticles motile density and concentration enhance due to a higher squeezing Reynolds number.

Chemical reactions relationships with mass transfer is very complex. This can be shown in the absorption and synthesis of reactant species at numerous rates of mass transfer. Chemical reactions find application in sciences and engineering, such as food processing and electric power generator. Shi et al. (2021) studied the significance of activation energy on bioconvection flow of magneto-cross nanofluid filled with gyrotactic microorganisms. They employed appropriate similarity variables to change their governing PDEs to ODEs. Their transformed ODEs were solved numerically by utilizing the shooting technique. They concluded that the activation energy greatly affects the species concentration. Puneeth et al. (2021) studied bioconvection of a radiating hybrid nanofluid with heterogeneous-homogeneous chemical reaction. Their flow equations were solved using the Runge-Kutta fourth-order technique. They concluded that heterogeneous reaction parameters give a significant effect on the concentration field. Waqas et al. (2021) examined bioconvection mass transport of micropolar nanofluid flow with thermal and exponentially spaced-based heat flux. Their flow equations were solved numerically, and they concluded that a higher thermophoresis parameter enriched the concentration profile. Mabood et al. (2017) studied radiation effects on melting heat transfer and stagnation point flow. Their transformed flow equations were solved numerically using the Runge-Kutta fourth-fifth order method. It was concluded in their study that temperature declines because of an increase in the melting parameter. Hayat et al. (2017) examined stretching rotating radiative flow with variable thickness. They solved their transformed equations by using Von Karman transformations. They concluded that a higher Prandtl number elevates the Nusselt number. Despite extensive studies on non–Newtonian and nanofluid dynamics, existing literature has major omissions concerning the combined effects of magnetic fields, variable thermophysical properties, and cross–diffusion phenomena in Williamson–type nanofluids. Hence, this study explores the variable viscosity, thermal conductivity, and Soret–Dufour mechanisms jointly influence MHD free convective of Williamson nanofluids over stretching sheets

Mathematical formulation

Consider a viscous, steady, incompressible, and laminar two-dimensional boundary layer motion of Williamson nanofluid across

a spreading surface. The physical properties of viscosity and thermal conductivity are assumed to vary within the boundary layer. The flow is subjected towards the x-axis along the stretching sheet, and the y-axis was assumed normal to it (see Figure 1). The concentration and temperature at the stretching wall are considered to be C_w and T_w while far away from the stretching wall are C_∞ and T_∞ as the concentration and temperature. The level of species concentration is assumed to be high such that Soret-Dufour mechanisms can not be neglected. A magnetic field of uniform strength with an inclined angle α was imposed in the opposite direction to the fluid flow. Based on the assumptions above, the equations that governed the fluid flow phenomena are:

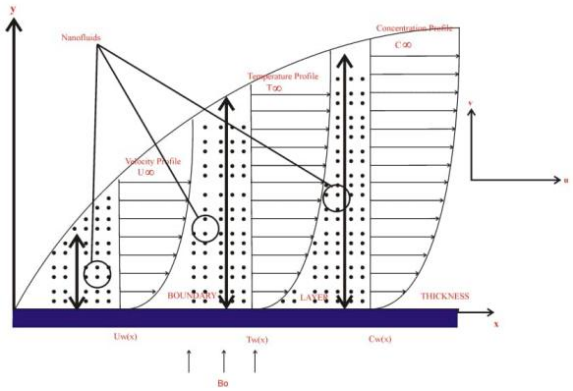

Figure 1: Model of physical coordinate system.

$$S = -pT + \tau \tag{1}$$

$$\tau = \left[\mu_\infty + \frac{(\mu_0 - \mu_\infty)}{1-\Gamma(\dot\gamma)}\right] A_1 \tag{2}$$

From which the pressure is p, I means Identity, τ is the stress tensor, μ_0 is zero along with an infinite shear rate and μ_∞, $\Gamma > 0$ signifies constant time, A_1 means the tensor of Rivlin-Erickson, and $\dot\gamma$ is given as:

$$\dot\gamma = \sqrt{\frac{1}{2}\pi}, \quad \text{where} \pi = \text{trace}(A_1^2) \tag{3}$$

$$\dot\gamma - \left[\left(\frac{\partial u}{\partial x}\right)^2 + \frac{1}{2}\left(\frac{\partial u}{\partial x} + \frac{\partial v}{\partial x}\right)^2 + \left(\frac{\partial v}{\partial y}\right)^2\right]^{\frac{1}{2}} = 0 \tag{4}$$

where π is the second invariant strain tensor. It should be noted in this study that the case when $\mu_\infty = 0$ and $\Gamma\dot\gamma < 1$ is considered. Hence, equation (1.2) is the extra stress tensor, which takes the form:

$$\tau = \left[\frac{\mu_0}{1-\Gamma\dot\gamma}\right] A_1 \tag{5}$$

Therefore, the extra stress tensor components shown in equations (3-5) are:

$$\tau_{xx} - 2\mu_0[1+\Gamma\dot\gamma]\frac{\partial u}{\partial x} = 0, \quad \tau_{xy} = \tau_{yx} = \mu_0[1+\Gamma\dot\gamma]\left(\frac{\partial u}{\partial y} + \frac{\partial v}{\partial x}\right)$$

$$\tau_{yy} = 2\mu_0[1+\Gamma\dot\gamma]\frac{\partial v}{\partial y}, \quad \tau_{xz} = \tau_{yz} = \tau_{zx} = \tau_{zy} = \tau_{xz} = 0 \tag{6}$$

Using Roseland approximation and following Alao et al. (2016), the radiative heat flux is given as:

$$q_r = -\frac{4\sigma_s}{3k_e}\frac{\partial T^4}{\partial y} \tag{7}$$

By using the Roseland approximation, the pseudoplastic fluid is restricted to a thin liquid. Taking the difference in the temperature within the flow domain to be small so that equation (7) above is linearized by simplifying T^4 using the Taylor series within T_∞ and neglecting higher-order terms:

$$T^4 \approx 4T_\infty^3 T - 3T_\infty^4 \tag{8}$$

Employing equations 1 - 6 and with all the assumptions above and the rheological equations of the Williamson fluid, the flow equations in this study are:

$$\frac{\partial u}{\partial x} + \frac{\partial v}{\partial y} = 0 \tag{9}$$

$$u\frac{\partial u}{\partial x} + v\frac{\partial u}{\partial y} = \frac{1}{\rho}\frac{\partial}{\partial y}\left(\mu\frac{\partial u}{\partial y}\right) - \frac{\sigma\beta(x)^2}{\rho}\sin\alpha u - \frac{u}{K}\frac{\mu(T)}{\rho} - \frac{1}{\rho}\frac{\Gamma}{\sqrt{2}}\frac{\partial}{\partial y}\left(\mu\left(\frac{\partial u}{\partial y}\right)^2\right) \tag{10}$$

$$u\frac{\partial T}{\partial x} + v\frac{\partial T}{\partial y} = \frac{1}{\rho c_p}\frac{\partial}{\partial y}\left(k\frac{\partial T}{\partial y}\right) + \frac{\mu(T)}{\rho c_p}\left[\left(\frac{\partial u}{\partial y}\right)^2 + \sqrt{2}\Gamma\left(\frac{\partial u}{\partial y}\right)^3\right] - \frac{1}{\rho c_p}\frac{\partial q_r}{\partial y} + \frac{D_m K_T}{c_s c_p}\frac{\partial^2 C}{\partial y^2} + \tau\left[D_B\frac{\partial T}{\partial y}\frac{\partial C}{\partial y} + \frac{D_T}{T_\infty}\left(\frac{\partial T}{\partial y}\right)^2\right] \tag{11}$$

$$u\frac{\partial C}{\partial x} + v\frac{\partial C}{\partial y} = D_m\frac{\partial^2 C}{\partial y^2} - K_1(C - C_\infty) + \frac{D_T}{T_\infty}\frac{\partial^2 T}{\partial y^2} - \frac{\partial}{\partial y}(V_T C) \tag{12}$$

subject to the constraints $u = u_w(x) = U_0(x+b)^m, \quad v = 0, \quad T = T_w, \quad C = C_w, \quad \text{at} y = (x+b)^{\frac{1-m}{2}}$

$$u = 0, \quad T = T_\infty, \quad C = C_\infty, \quad \text{as} y \to \infty \tag{13}$$

In equation (1.12), the thermophoretic V_T is given as:

$$V_T = -k_V\frac{\nu T}{T_{ref}} = \frac{k_V}{T_{ref}}\frac{\partial T}{\partial y} \tag{14}$$

where k–thermophoretic coefficient defined as

$$k = 2c_s\left(\frac{\lambda_g}{\lambda_p} + C_t k_n\right)\left[1 + k_n(C - 1 + C_2\exp(-\frac{c_s}{k_n}))\right]\left((1+3C_m k_n)(1+2\frac{\lambda_g}{\lambda_p} + 2C_t k_n)\right)^{-1} \tag{15}$$

where C_1, C_2, C_3, C_m, c_s and C_t are constant, λ_g and λ_p signifies thermal conductivities of both liquid and diffused particles, k_n signifies Knudsen number. The fluid thermal conductivity $k(T)$ together with variable viscosity $\mu(T)$ are given in the form:

$$k = k_\infty[1+\xi\theta], \quad \mu = \mu_\infty[1+\xi\theta] \tag{16}$$

where the value of ξ is taken to be very small, k_∞ signifies the conductivity of the liquid far from the sheet. Note that

$$\frac{1}{\mu} = \frac{1}{\mu_\infty}[1+\gamma(T-T_\infty)], \quad i.e \quad \frac{1}{\mu} = a(T - T_r) \tag{17}$$

where $a = \frac{\gamma}{\mu_\infty}$, $T_r = T_\infty - \frac{1}{\gamma}$ and $\psi(x,y)$ signifies stream function given as $u = \frac{\partial\psi}{\partial y}$ and $v = -\frac{\partial\psi}{\partial x}$. The following similarity transformation is introduced on the governing equations (1.9)-(1.13)

https://dx.doi.org/10.4314/swj.v20i4.15

$$\frac{\eta}{y(x+b)^{\frac{m-1}{2}}}\sqrt{\frac{U_0(m+1)}{2\nu}}=0,\quad \frac{\psi(x,y)}{(x+b)^{\frac{m+1}{2}}}f-\sqrt{\frac{2\nu U_0}{m+1}}=0$$

$$\theta(\eta)=\frac{(T-T_\infty)}{(T_w(x)-T_\infty)},\quad \phi(\eta)=\frac{(C-C_\infty)}{(C_w(x)-C_\infty)} \tag{18}$$

Substituting equation (1.8) above into the definition of the stream function, we obtain

$$\frac{u}{U_0(x+b)^m}=f'(\eta),\quad \frac{v}{f'(\eta)\eta\left(\frac{m-1}{m+1}\right)}=\sqrt{\frac{m+1}{2}\nu U_0(x+b)^{m-1}}\frac{\sqrt{\frac{m+1}{2}\nu U_0(x+b)^{m-1}}f(\eta)}{f'(\eta)\eta\left(\frac{m-1}{m+1}\right)} \tag{19}$$

The transformed equations now become:

$$f'''-\left(\frac{2}{Po(m+1)}\right)f'=\frac{\theta_r-\theta}{\theta_r}\left[f''-\left(\frac{2m}{m+1}\right)f^2-M^2\sin^2(\alpha)f'-\beta f'f''\right]+\frac{1}{\theta_r-\theta}[\theta f''+\xi\theta f''^2] \tag{20}$$

$$\theta''=\frac{1}{1+s\theta}\left[Pr\left(\frac{1-m}{m+1}\right)f'\theta-f\theta'-Ecf'^2+\frac{\theta_r Ec}{(\theta_r-\theta)}(f'')^2-\beta(f''^3)\right]-s\theta^2-R\theta''-Na\theta'\phi'+Nt\theta' \tag{21}$$

$$\frac{1}{Sc}\phi''-Kr\phi+f\phi'+Sr\theta''+\tau[\theta'\phi'+\phi\theta'']=0 \tag{22}$$

subject to:

$$f=\chi\left[\frac{1-m}{m+1}\right],\quad f'=1,\quad \theta=1,\quad \phi=1,\quad \text{as}\eta=0 \tag{23}$$

$$f'\to 0,\quad \theta\to 0,\quad \phi\to 0,\quad \text{as}\eta\to\infty \tag{24}$$

where

$$Sc=\frac{\nu}{D},\quad Kr=\frac{2K_1}{u_0(m+1)(x+b)^{m-1}},\quad Sr=\frac{D_T(T_w-T_\infty)}{T_\infty(C_w-C_\infty)},\quad \tau=\frac{k\nu}{T_{ref}}\frac{(T_w-T_\infty)}{\sqrt{2}}(x+b)^m$$

are Schmidt number, chemical reaction parameter, Soret number, and thermophoresis parameter.

MATERIALS AND METHODS

To solve equations (20), (21), and (22) subject to (23) and (24), we first determine all initial conditions. Once the initial conditions are found, we solve the equations (20), (21), and (22) subject to (23) and (24) using the Runge-Kutta fourth-order method with a successive iterative step length of 0.01. The non-dimensional velocity and temperature profiles are shown in Figures 2-15 for various values of different physical parameters. To validate the employed method, the authors have compared the results of $f''(0)$ with published work. These comparisons are given in Table 1 and show very good agreement. We proceed by writing the transformed equations for each case in first-order ODEs as follows:

$$f=\alpha_1,\quad \frac{df}{d\eta}=\frac{d\alpha_1}{d\eta}=\alpha_2,\quad \frac{d^2f}{d\eta^2}=\frac{d}{d\eta}\left(\frac{df}{d\eta}\right)=\frac{d\alpha_2}{d\eta}=\alpha_3,\quad \frac{d^3f}{d\eta^3}=\frac{d}{d\eta}\left(\frac{d^2f}{d\eta^2}\right)=\frac{d\alpha_3}{d\eta}$$

$$\theta=\alpha_4,\quad \frac{d\theta}{d\eta}=\frac{d\alpha_4}{d\eta}=\alpha_5,\quad \frac{d^2\theta}{d\eta^2}=\frac{d}{d\eta}\left(\frac{d\theta}{d\eta}\right)=\frac{d\alpha_5}{d\eta}$$

$$\phi=\alpha_6,\quad \frac{d\phi}{d\eta}=\frac{d\alpha_6}{d\eta}=\alpha_7,\quad \frac{d^2\phi}{d\eta^2}=\frac{d}{d\eta}\left(\frac{d\phi}{d\eta}\right)=\frac{d\alpha_7}{d\eta}$$

Substituting these first-order ODEs into (20), (21), and (23), we obtain:

$$\frac{d\alpha_3}{d\eta}=\left(\frac{2}{Po(m+1)}\right)\alpha_2=\frac{\theta_r-\alpha_4}{\theta_r}\left[\alpha_1\alpha_3-\left(\frac{2m}{m+1}\right)(\alpha_2)^2-M^2\sin^2(\alpha)\alpha_2-\beta\alpha_3\frac{d\alpha_3}{d\eta}\right]+\frac{1}{\theta_r-\alpha_4}[\alpha_5\alpha_3+\beta\alpha_5(\alpha_3)^2]$$

$$\frac{d\alpha_5}{d\eta}=\frac{1}{1+s\alpha_4}\left[Pr\left(\frac{1-m}{m+1}\right)\alpha_2\alpha_4-\alpha_1\alpha_5-Ec(\alpha_3)^2+\frac{\theta_r}{\theta_r-\alpha_4}Ec(\alpha_3)^2-\beta(\alpha_3)^3-Nb\alpha_5\alpha_7\right]-Nt(\alpha_5)^2-s(\alpha_5)^2-R\frac{d\alpha_5}{d\eta}$$

$$\frac{d\alpha_7}{d\eta}-Sc\alpha_1\alpha_7-ScKr\alpha_6+ScSr\frac{d\alpha_5}{d\eta}+Sc\tau\alpha_5\alpha_7+Sc\tau\alpha_6\frac{d\alpha_5}{d\eta}=0$$

Also,

$$\frac{d\alpha_3}{d\eta}\left(\frac{2}{Po(m+1)}\right)\alpha_2=\frac{\theta_r-\alpha_4}{\theta_r}\alpha_1\alpha_3-\frac{\theta_r-\alpha_4}{\theta_r}\left(\frac{2m}{m+1}\right)(\alpha_2)^2-\frac{\theta_r-\alpha_4}{\theta_r}M^2\sin^2(\alpha)\alpha_2-\frac{\theta_r-\alpha_4}{\theta_r}\beta\alpha_3\frac{d\alpha_3}{d\eta}=\frac{1}{\theta_r-\alpha_4}[\alpha_3\alpha_3+\beta E\alpha_3(\alpha_3)^2]$$

$$\frac{d\alpha_5}{d\eta}+R\frac{d\alpha_5}{d\eta}=\frac{1}{1+s\alpha_4}\left[Pr\left(\frac{1-m}{m+1}\alpha_2\alpha_4-\alpha_1\alpha_5-Ec(\alpha_3)^2\right)+\frac{\theta_r}{\theta_r-\alpha_4}Ec(\alpha_3)^2-\beta(\alpha_3)^3-Nb\alpha_3\alpha_7-Nt(\alpha_3)^2-s(\alpha_3)^2\right]$$

$$\frac{d\alpha_7}{d\eta}=Sc\alpha_1\alpha_7+Sckr\alpha_6-Sc\tau\alpha_5\alpha_7-(ScSr+Sc\tau\alpha_6)\frac{d\alpha_5}{d\eta}$$

Simplifying further to obtain:

$$\frac{d\alpha_3}{d\eta}\left[1+\frac{\theta_r-\alpha_4}{\theta_r}\beta\alpha_3\right]=\frac{\theta_r-\alpha_4}{\theta_r}\alpha_1\alpha_3-\frac{\theta_r-\alpha_4}{\theta_r}\left(\frac{2m}{m+1}\right)(\alpha_2)^2-\frac{\theta_r-\alpha_4}{\theta_r}M^2\sin^2(\alpha)\alpha_2+\frac{1}{\theta_r-\alpha_4}\alpha_3\alpha_3+\frac{1}{\theta_r-\alpha_4}\beta E\alpha_3(\alpha_3)^2$$

$$\frac{d\alpha_5}{d\eta}\left[1+\frac{R}{1+s\alpha_4}\right]=\frac{1}{1+s\alpha_4}\left[Pr\left(\frac{1-m}{m+1}\alpha_2\alpha_4-\alpha_1\alpha_5-Ec(\alpha_3)^2\right)+\frac{\theta_r}{\theta_r-\alpha_4}Ec(\alpha_3)^2\right.$$

Science World Journal Vol. 20(No 4) 2025 https://dx.doi.org/10.4314/swj.v20i4.15
www.scienceworldjournal.org
ISSN: 1597-6343 (Online), ISSN: 2756-391X (Print)
Published by Faculty of Science, Kaduna State University

$$-\beta(\alpha_3)^3 - Nb\alpha_3\alpha_7 - Nt(\alpha_3)^2 - s(\alpha_3)^2]$$

Now substituting equation above:

$$\frac{d\alpha_7}{d\eta} = Sc\alpha_1\alpha_7 + Sckr\alpha_6 - Sc\tau\alpha_5\alpha_7 - (ScSr + Sc\tau\alpha_6)A$$

where,

$$A = \frac{1}{1+s\alpha_4}\left[Pr\left(\frac{1-m}{m+1}\alpha_2\alpha_4 - \alpha_1\alpha_5 - Ec(\alpha_3)^2\right) + \frac{\theta_r}{\theta_r - \alpha_4}Ec(\alpha_3)^2 - \beta(\alpha_3)^3 - Nb\alpha_3\alpha_7 - Nt(\alpha_3)^2 - s(\alpha_3)^2\right] \times \left[1 + \frac{R}{1+s\alpha_4}\right]^{-1}$$

RESULTS AND DISCUSSION

The reduced equations (20)-(22), along with the boundary conditions (23) and (24) are highly coupled nonlinear ordinary differential equations. This set of equations has been solved by utilizing the Runge-Kutta method alongside the shooting technique. With the numerical results, the contribution of each parameter is presented graphically. In the same vein, the computational outcomes of flow parameters on engineering interest are presented in tabular form.

Table 1. Computational values for skin friction coefficient (Cf), Nusselt number (Nu), and Sherwood number (Sh) for different values of flow parameters

P	θr	M	β	S	Pr	Ec	R	Sc	kr	Cf	Nh	Sh
0.3										1.6918	1.6084	0.1306
1.6										1.7309	1.5544	0.1306
0.9										1.8339	1.3214	0.1306
	2.0									2.6421	1.4850	0.1234
	4.0									2.9753	2.4220	0.1234
	6.0									3.1475	3.9971	0.1234
		0.0								1.0263	1.5682	0.1323
		0.5								1.0124	1.5184	0.1323
		1.0								1.0020	1.5149	0.1323
			0.1							1.8980	1.6125	0.1487
			0.3							1.6577	1.6125	0.1487
			0.5							1.5112	1.6125	0.1487
				1.0						1.2173	0.5778	0.5171
				2.0						1.1159	0.5912	0.5171
				3.0						1.1141	0.6001	0.5171
					0.71					1.0397	1.0693	0.3095
					1.00					1.3843	1.1104	0.3095
					3.00					1.4812	1.5205	0.3095
						0.2				1.6227	0.4181	0.4561
						0.4				1.5660	0.3228	0.4561
						0.6				1.5094	0.2123	0.4561

Table 4.1 shows the values of Cf, Nu, and Sh for controlling parameters such as Po, θr , M, β , s, Pr, and Pr. An increment in the value of Po is seen to enhance Cf and degenerate Nu in T Increase in the value of θr is observed to elevate the value of Cf and Nu. This implies that an increase in θr speed up the rate of heat transport. A large value of M is noticed to drastically decrease Cf and Nu. This is a result of the Lorentz force produced by an increase in M. Also, an increase in the value of β is noticed to degenerate Cf. This is due to the imposed magnetic field on the flow, an increase in the value of s is observed in the speed rate of the heat transport due to the increase in the value of Nu. It is clearly noticed that a large value of Pr is noticed to enhance Cf and Nu, but has negligible on Sh. An increase in the value of Ec is observed to elevate Cf and Nu.

Science World Journal Vol. 20(No 4) 2025 https://dx.doi.org/10.4314/swj.v20i4.15
www.scienceworldjournal.org
ISSN: 1597-6343 (Online), ISSN: 2756-391X (Print)
Published by Faculty of Science, Kaduna State University

Table 2 Computational values for skin friction coefficient (Cf), Nusselt number (Nu), and Sherwood number (Sh) for different values of flow parameters.

R	Sc	Kr	Cf	Nh	Sh
0.5			1.6470	0.3172	0.5111
1.0			1.6793	0.5631	0.5111
2.0			1.7266	0.7235	0.5111
	0.22		1.6793	0.3632	0.4124
	0.61		1.5341	0.3632	0.4012
	1.00		1.4233	0.3632	0.3900
		0.3	1.6990	0.2632	0.5312
		0.5	1.6793	0.2632	0.6124
		0.7	1.6595	0.2632	0.6459

Table 3 Shows the validation of the present outcomes with those of Ahmed et al. (2020) when Θ_r = s = B = R = Kr = T = X = 0. The present outcomes are found to be correct in Table 4.3
Flow Parameters Ahmed et al. (2020) Present outcomes

Sr	**Ec**	**Pr**	**Sc**	**Cf**	**Nh**	**Sh**	**Cf**	**Nh**	**Sh**
0.1				0.4915	0.5050	0.5708	0.4913	0.5048	0.5706
0.5				0.5137	0.4760	0.5786	0.5135	0.4758	0.5784
2.0				0.5369	0.4472	0.5866	0.5367	0.4470	0.5864
	0.01			0.9756	0.7319	0.9548	0.9754	0.7317	0.9546
	0.1			0.9838	0.6504	0.7649	0.9836	0.6502	0.9647
	0.2			0.9946	0.5586	0.9764	0.9944	0.5584	0.9762
		0.71		0.9743	0.7318	0.9547	0.9741	0.7316	0.9545
		1.0		0.9284	0.9041	0.9304	0.9282	0.9039	0.9302
		7.0		0.5383	3.5086	0.6012	0.5381	3.5084	0.6010
			0.22	1.2235	0.9366	0.5156	1.2233	0.9364	0.5154
			0.61	1.0835	0.7162	1.0260	1.0833	0.7160	1.0258
			1.0	0.9913	0.6043	1.3792	0.9911	0.6041	1.3790

Figure 2 represents the significance of the Williamson parameter (β) on the velocity profile. A higher value of β is detected to enhance the velocity profile. Practically, in a scenario of constant viscosity and thermal conductivity, that is $s = \epsilon = 0$, there is a boost in velocity within the boundary layer. The assumption of constant viscosity and thermal conductivity in a moving fluid is unrealistic. Hence, the present analysis examines the thermal conductivity and viscosity to vary within the stretching surface. Physically, raising the value of β along with variable viscosity and thermal conductivity helps in enhancing the fluid velocity.

Figure 3 shows the significance of the chemical reaction parameter (kr) on the velocity as well as concentration profiles. A higher value of kr is detected to deteriorate both velocity and concentration profiles. This shows a corrosive reaction in the fluid within the boundary layer. However, the chemical reaction on the fluid nanoparticles shows a destructive reaction by decreasing the velocity and concentration profiles.

Figure 4 depicts the effect of the magnetic field parameter (M) on the velocity profile. A higher value of M was detected to deteriorate the velocity distribution. The presence of the magnetic field parameter in this analysis gave rise to the Lorentz force. Physically, the Lorentz force possesses more strength with a higher value of M and thereby causes a reduction in the velocity of the fluid.

Figure 5 represents the impact of the Brownian motion parameter (Nb) on the velocity and temperature profiles. It is observed that an increase in Nb causes a reduction in the velocity and temperature profiles. This is due to the Lorentz force produced as a result of imposing the magnetic field transversely to the flow direction.

Figure 6 illustrates the impact of the nanofluid thermophoresis

Science World Journal Vol. 20(No 4) 2025 https://dx.doi.org/10.4314/swj.v20i4.15
www.scienceworldjournal.org
ISSN: 1597-6343 (Online), ISSN: 2756-391X (Print)
Published by Faculty of Science, Kaduna State University

parameter (Nt) on the velocity and temperature profiles. A higher value of Nt is observed to decrease the temperature and increase the velocity profile. Nanofluid thermophoresis is a scenario that explains the migration of microparticles towards a degenerating thermal gradient. Physically, Figure 6 indicates that the microparticles diffuse from the hot surface towards a cold surface. Hence, there is a rise in the fluid velocity within the cold surface with reduced temperature.

Figure 7 represents the effect of the Prandtl number (Pr) on the velocity and temperature profiles. A decrease in the velocity and temperature profile is detected due to a higher value Pr. Pr demonstrates the relationship existing between the thermal conductivity and kinematic viscosity. This means that Pr controls the thickening of thermal and momentum boundary layers when considering heat and mass transfer phenomena. Therefore, a very small Pr possesses very high heat conductivities while the structure of the thermal layer becomes very thick. Due to this, raising Pr in the heat transfer process reduces the hydrodynamic and thermal layers.

Figure 8 illustrates the significance of the thermal radiation parameter (R) on the velocity and temperature profiles. A higher value of R is detected to enhance the velocity and temperature profiles. Thermal radiation is of great importance in thermal engineering scenarios where the temperature is very high. It is finalized in this analysis that R is important when $R \neq 0$. Due to variable viscosity and thermal conductivity, the environment within the layer becomes very hot.

Figure 9 shows the effect of the Schmidt number on the velocity and concentration profiles. A decrease in velocity and concentration profiles is noticed due to a higher Schmidt number. The Schmidt number is the ratio of fluid kinematic viscosity to fluid mass diffusivity. Physically, kinematic viscosity (ν) $>$ mass diffusivity means that the Schmidt number is very high. Hence, the rate of mass transfer is reduced due to the significance of concentration buoyancy effects.

Figure 10 illustrates the effect of variable viscosity on the velocity and temperature profiles. In reality, any fluid in motion cannot possess a constant viscosity. The viscosity is noted for causing resistance to fluid flow within the boundary layer. A higher value of variable viscosity in Figure 10 shows a reduction in the velocity and temperatures. Hence, the thickness of the hydrodynamic and thermal boundary layer reduces. Figure 11 shows the impact of the thermophoresis parameter (τ) on the velocity and concentration profiles. A higher value of τ is detected to cause an increase in the species concentration as well as velocity distributions.

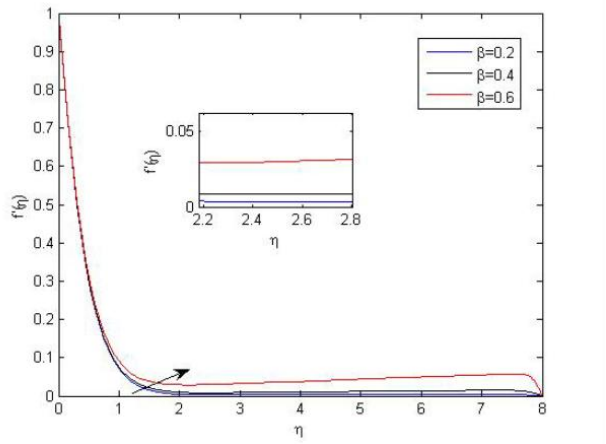

Figure 2: Effect of Williamson parameter on the velocity profile.

(a)

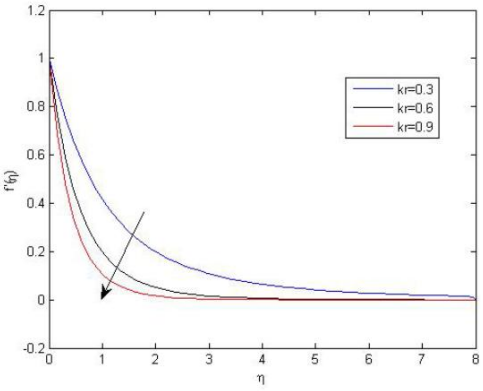

(b)

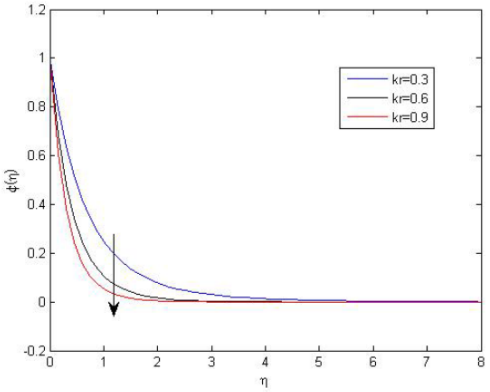

Figure 3: Effect of chemical reaction parameter on the velocity and concentration profiles.

Science World Journal Vol. 20(No 4) 2025 https://dx.doi.org/10.4314/swj.v20i4.15
www.scienceworldjournal.org
ISSN: 1597-6343 (Online), ISSN: 2756-391X (Print)
Published by Faculty of Science, Kaduna State University

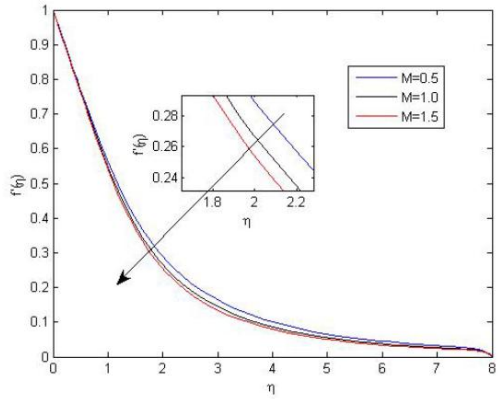

Figure 4: Effect of magnetic parameter on the velocity profile.

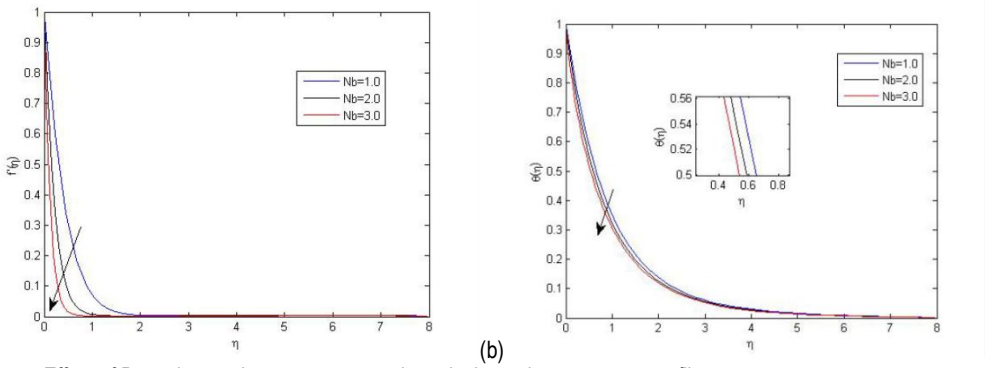

(a) (b)

Figure 5: Effect of Brownian motion parameter on the velocity and temperature profiles.

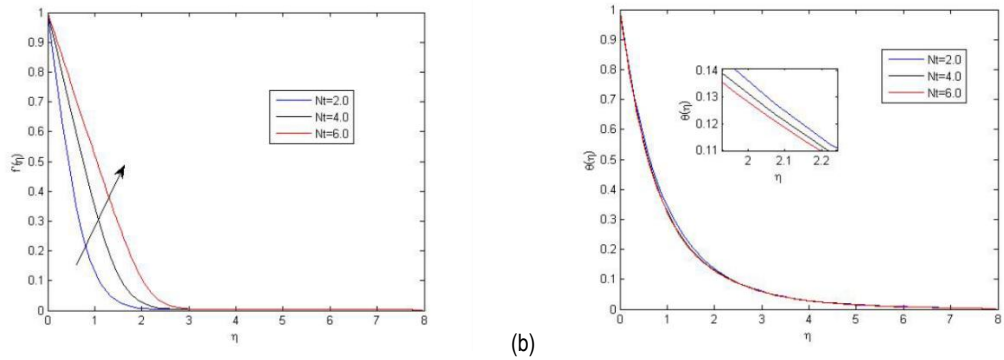

(a) (b)

Figure 6: Effect of nanofluid thermophoresis parameter on the velocity and temperature profiles.

Science World Journal Vol. 20(No 4) 2025 https://dx.doi.org/10.4314/swj.v20i4.15
www.scienceworldjournal.org
ISSN: 1597-6343 (Online), ISSN: 2756-391X (Print)
Published by Faculty of Science, Kaduna State University

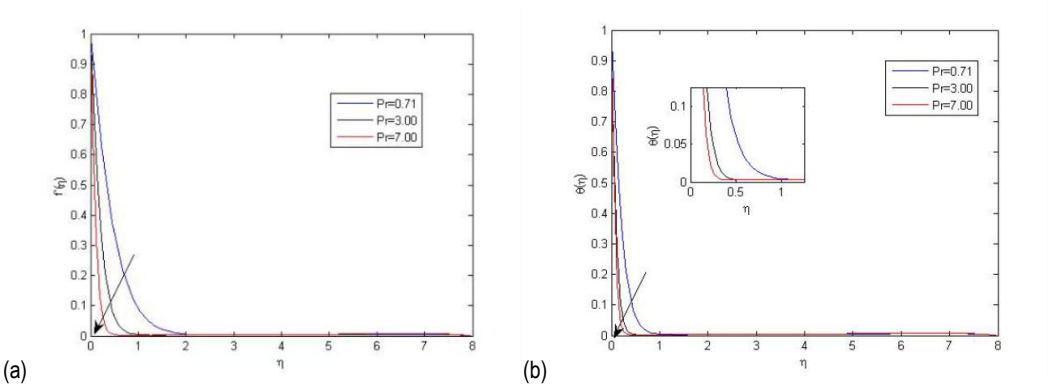

(a) (b)

Figure 7: Effect of Prandtl number on the velocity and temperature profiles.

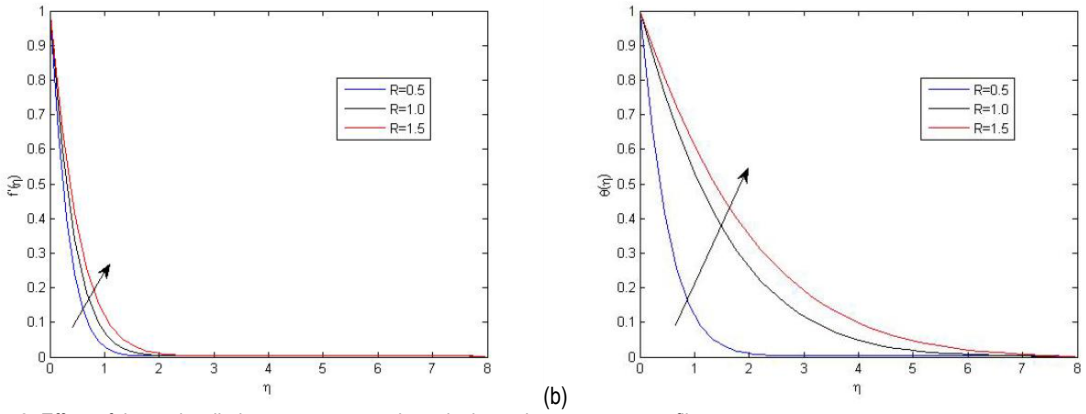

(a) (b)

Figure 8: Effect of thermal radiation parameter on the velocity and temperature profiles.

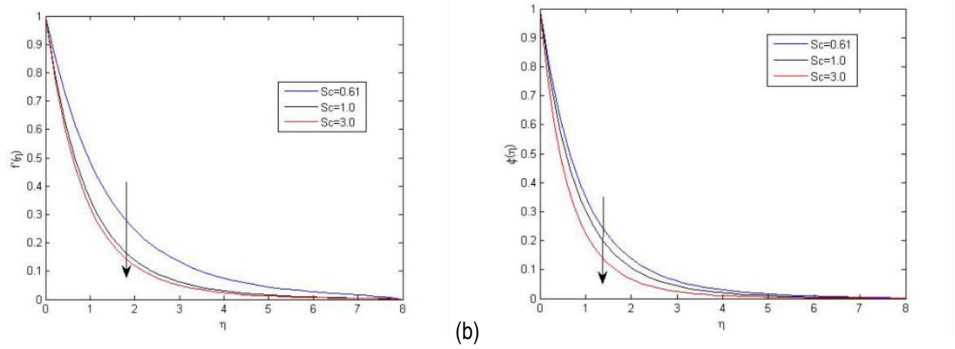

(a) (b)

Figure 9: Effect of Schmidt number on the velocity, and concentration profiles.

Science World Journal Vol. 20(No 4) 2025 https://dx.doi.org/10.4314/swj.v20i4.15
www.scienceworldjournal.org
ISSN: 1597-6343 (Online), ISSN: 2756-391X (Print)
Published by Faculty of Science, Kaduna State University

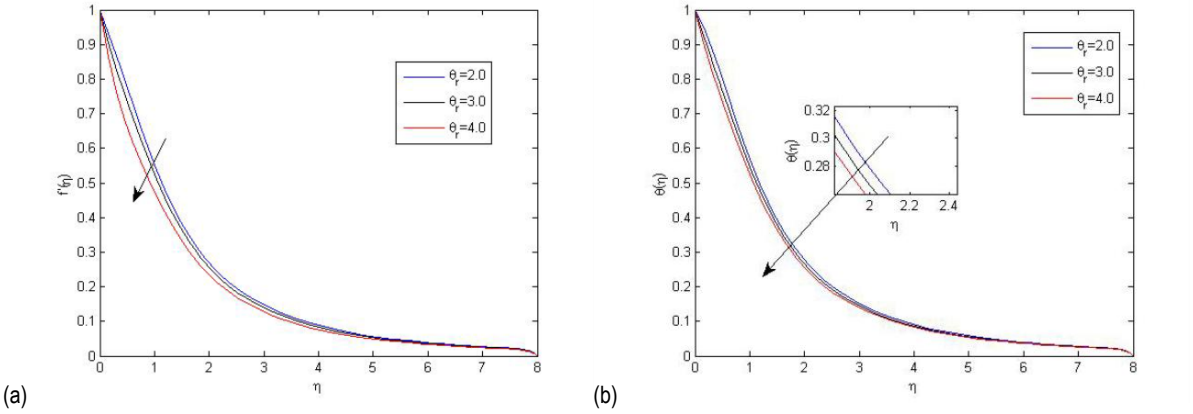

Figure 10: Effect of variable viscosity parameter on the velocity and temperature profiles.

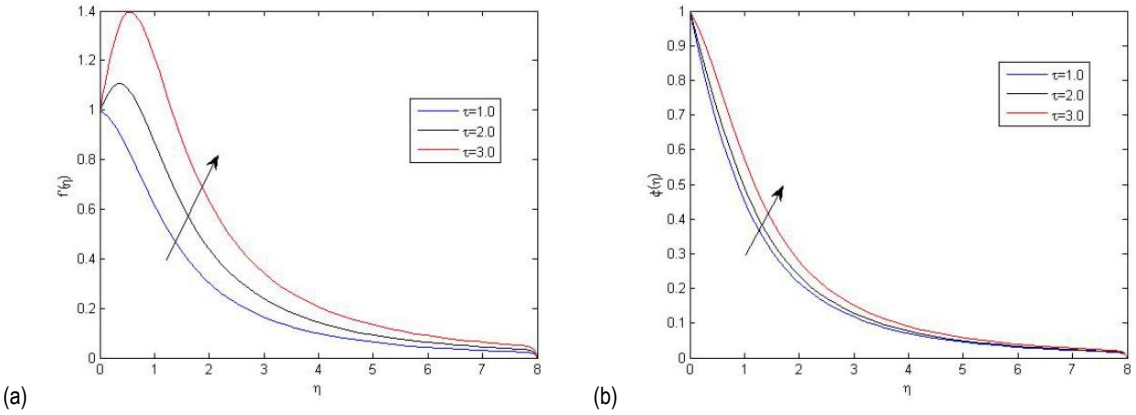

Figure 11: Effect of thermophoresis parameter on the velocity and concentration profiles.

Conclusion

The problem examined the significance of nanofluid in the systematic flow of Williamson fluid over a stretching surface. The thermophysical properties of the fluid were considered to vary within the boundary layer. The Runge-Kutta method, along with the shooting technique, was employed to solve the system of transformed ODEs. The physical outcomes for various flow parameters were presented graphically to explain the physics of the problem. The major findings are:

1) An increase in the Williamson parameter enhances the fluid velocity along with the thickness of the hydrodynamic boundary layer.
2) The application of a magnetic field in the flow direction generates a Lorentz force that decreases the fluid velocity.
3) The Brownian motion parameter was observed to reduce the velocity of the fluid while increasing the temperature and concentration boundary layer thickness.
4) Thermophoresis was found to influence particle deposition, leading to a change in concentration distribution within the fluid.

Nomenclature

A - Constant
A_1 - First Rivlin –Erikson tensor
Bo – Magnetic field ($Kgs^{-2}\ A^{-1}$)
C - Dimensional Concentration (mol/m^3)
C_p - Specific heat at constant Pressure (Unit: $Jkg^{-1}\ k^{-1}$]
C_∞ - Concentration at free stream (mol/m^3)
D - Mass diffusivity (m^2/S)
D_B - Browman motion coefficient (m^2/s)
D_m - Mass diffusivity
I - Identity
K = Thermal Conductivity
K_1= Chemical reaction
k = Porosity term
k^* - Mean absorption coefficient
K_T - Thermal diffusivity ratio
k(T)-Thermal conductivity (w/mK)
K_n - Knudsen number
k_∞ - Conductivity of fluid far away from sheet
N_{ux} - Nusselt number
p - Pressure (Pa)
qr = radiative heat flux (w/m^2)
R - radiation parameter

S - Stress tensor
Sh_x - Sherwood number
T - Fluid temperature (kelvin)
T_∞ - temperature of free stream
U - velocity component in x - direction (m/s)
U_w- stretchg in sheet velocity
U_∞ - velocity at free stream (m/s)
V - velocity component s in y - direction (m/s)
V_w - velocity at wall (m/s)
V_T - Thermophoresis velocity (m/s)

Greek Alphabets

Γ- time constant
μ- dynamic viscosity
μ(τ)-Variable viscosity
μ_∞ Velocity at free stream
μ_0 Limiting viscosity at zero shear rate
σ^*- Stefan-boltzmann constant
θ - Dimensionless temperature
ρ - Fluid density [unit;Kg/m^2]
ν- Kinematic viscosity [unit m^2/s]
σ - Electrical conductivity fluid (unit: mΩ/m)
ψ - stream function
τ - Brownian motion parameter

REFERENCES

Ahmed L.O., Falodun B.O., & Abdulwaheed J (2020). Mechanism of Soret – Dufour Magnetohydrodynamics, heat and mass transfer flow with buoyancy force, and viscous dissipation effects. Heat transfer,2020; 1- 18. https://doi.org/10.1002/htj.21748

Akolade M, T., Adeosun, T, A, & Olabode J.O. (2021), Influence of Thermophysical Features on MHD Squeezed Flow of Dissipative Casson Fluid with Chemical and Radiative Effects, J. Appl. Comput. Mech., 7(4) (2021) 1999-2009 DOI: 10.22055/JACM.2020.34909.2508

Alao F.I., Fagbade A.I.,& Falodun B.O. (2016), Effects of thermal radiation, Soret and Dufour on an unsteady heat and mass transfer flow of a chemically reacting fluid past a semi-infinite vertical plate with viscous dissipation, Journal of the Nigerian Mathematical Society 35 (2016) 142-158.

Alhussain Z. A., Renuka, A. & Muthtamilselvan, M. (2021), A magneto-bioconvective and thermal conductivity enhancement in nanofluid flow containing gyrotactic microorganism, Case Studies in Thermal Engineering 23, 100809, 1-14. Available online 15 December 2020 214-157X/ 2020 (http://creativecommons.org/licenses/by-nc-nd/4.0/).

Ali M.E & Sandeep N (2017), Cattaneo-Christov model for radiative heat transfer of magnetohydrodynamic Casson-ferrofluid: A numerical study, Results in Physics 7 (2017) 21-30.

Alzahrani, F, & Ijaz, K M. (2021), Significance of induced magnetic force bioconvective flow of radiative Maxwell Nanofluid with activation energy, Case Studies in Thermal Engineering 27 (2021) 101282, 1-10.

Alzahrani A, K, Malik Z, U, Ali S,A,& Taza G (2021), Hybrid nanofluid flow in a Darcy-Forchheimer permeable medium over a flat plate due to solar radiation, Case Studies in Thermal Engineering 26 (2021) 100955, 1-12.

Arain, M. B., Bhatti, M. M., Zeeshan, A. & Alzahrani, F. S. (2021). Bioconvection Reiner-Rivlin Nanofluid Flow between Rotating Circular Plates with Induced Magnetic Effects, Activation Energy and Squeezing Phenomena. Mathematics 2021, 9, 2139. https://doi.org/10.3390/math9172139doi:10.3390/math9172139.

El-Zahar, E.R.; Mahdy, A.E.N.; Rashad, A.M.; Saad,W.; & Seddek, L.F(2021). Unsteady MHD Mixed Convection Flow of Non-Newtonian Casson Hybrid Nanofluid in the Stagnation Zone of Sphere Spinning Impulsively. Fluids 2021, 6, 197. https://doi.org/10.3390/fluids6060197doi:10.3390/fluids6060197.

Hafeez, M.B.; Sumelka,W.; Nazir, U.; Ahmad, H. & Askar, S.(2021), Mechanism of Solute and Thermal Characteristics in a Casson Hybrid Nanofluid Based with Ethylene Glycol Influenced by Soret and Dufour Effects. Energies 2021, 14, 6818. https://doi.org/10.3390/en14206818.

Hassan, W, Metib, A, Muhammad, T, & Khan, M, A (2021), Bioconvection transport of magnetized Walter's B nanofluid across a cylindrical disk with nonlinear radiative heat transfer, Case Studies in Thermal Engineering 26 (2021) 101097, 1-11

Hassan, W, Khan, S,A, & Muhammad, T (2022), Thermal analysis of magnetized flow of AA7072-AA7075/blood-based hybrid nanofluids in a rotating channel, Alexandria Engineering Journal (2022) 61, 3059-3068

Hussain, A, Qusain , H, Aysha ,R, Malik, M. Y, Nadeem, S & Hussain, S (2021), Heat Transport Improvement and Three-Dimensional Rotating Cone Flow of Hybrid-Based Nanofluid, Mathematical Problems in Engineering Volume 2021, Article ID 6633468, 11 pages https://doi.org/10.1155/2021/6633468

Hayat, T., Anum, S, Alsaedi, A., & Asghar, S (2015). Effect of inclined magnetic field in flow of third grade fluid with variable thermal Conductivity, AIP Advances 5, 087108 (2015); doi: 10.1063/1.4928321, pp 1-16

Hayat T, Sumaira Q, Maria I, &Ahmed, A. (2017), Radiative flow due to stretchable rotating disk with variable thickness, Results in Physics 7 (2017) 156-165

Kumar, R. Sood, S, Raju, C.S.K., & Shehzad S.A. (2018), Hydromagnetic unsteady slip stagnation flow of nanofluid with suspension of mixed bio-convection, Propulsion and Power Research 2019;8(4):362e372

Mabood, F, Shafiq, A., Hayat, T., & Abelman, S (2017). Radiation effects on stagnation point flow with melting heat transfer and second order slip, Results in Physics 7 (2017) 31-42

Mutuku-Njane W, N & Makinde, O, D (2013), Combined Effect of Buoyancy Force and Navier Slip on MHD Flow of a Nanofluid over a Convectively Heated Vertical Porous Plate, The ScientificWorld Journal Volume 2013, Article ID 725643, 8 pages http://dx.doi.org/10.1155/2013/725643.

Nayak, M.K., Shaw, S., Hassan, W, Makinde, O.D., Metib A, & Muhammad, T. (2021), Comparative study for magnetized flow of nanofluids between two parallel

permeable stretching/shrinking surfaces, Case Studies in Thermal Engineering 28 (2021) 101353, 1-18

Nisar KS, Khan U, Zaib A, Khan I & Baleanu D, (2020), Numerical Simulation of Mixed Convection Squeezing Flow of a Hybrid Nanofluid Containing Magnetized Ferroparticles in 50%:50% of Ethylene Glycol-Water Mixture Base Fluids Between Two Disks With the Presence of a Non-linear Thermal Radiation Heat Flux. Front. Chem. 8:792. doi: 10.3389/fchem.2020.00792

Onwubuoya C & Dada M.S (2021). Soret, viscous dissipation, and thermal radiation effects on MHD free convective flow of Williamson liquid with variable viscosity and thermal conductivity, Heat Transfer. 2021;50:4039–4061. DOI: 10.1002/htj.22063

Puneeth, V., Manjunatha, S., Makinde, O.D. & Gireesha, B.J. (2021), Bioconvection of a Radiating Hybrid Nanofluid Past a Thin Needle in the Presence of Heterogeneous-Homogeneous Chemical Reaction, Journal of Heat Transfer, 2021, Vol. 143 / 042502-1, 1-18.

Ramzan M, Dawar A, Saeed A, Kumam P, Watthayu W, & Kumam, W (2021). Heat transfer analysis of the mixed convective flow of magnetohydrodynamic hybrid nanofluid past a stretching sheet with velocity and thermal slip conditions. PLoS ONE 16(12): e0260854. https:// doi.org/10.1371/journal.pone.0260854.

Saeed A, Alghamdi W, Mukhtar S, Shah SIA, Kumam P, & Gul T (2021) Darcy-Forchheimer hybrid nanofluid flow over a stretching curved surface with heat and mass transfer. PLoS ONE 16(5): e0249434. https://doi.org/10.1371/journal.pone.0249434

SP Pallavi, MB Veena, Jagadish .V. Tawade, Nitiraj Kulkarni, Sami Ullah Khan, M. Tears, Manish Gupta, & Saja Abdulrahman Althobaiti (2024), Effects of exponentially stretching sheet for MHD Williamson nanofluid with chemical reaction and thermal radiative.Partial Differential Equations in Applied Mathematics 12(2024)1

Shi QH, Aamir, H, Ijaz K, Naveen K, R, Punith R, J, Prasannakumara, BC, Shah, NA, Khan, SU & Chung, JD (2021), Numerical study of bioconvection flow of magneto?cross nanofluid containing gyrotactic microorganisms with activation energy, Scientific Reports | (2021) 11:16030 | https://doi.org/10.1038/s41598021-95587-2

Tarakaram, N., & S. (1999).Shi Q.H., Aamir, H, Ijaz K, Naveen K, R, Punith R, J, Prasannakumara, B.C, Shah, N.A, Khan, S.U & Chung, J.D (2021), Numerical study of bioconvection flow of magneto cross nanofluid containing gyrotactic microorganisms with activation energy, Scientific Reports (2021) 11:16030 https://doi.org/10.1038/s41598-021-95587-2

Tarakaramu, N, & Satya N, P.V. (2019), Chemical Reaction Effects on BioConvection Nanofluid flow between two Parallel Plates in Rotating System with Variable Viscosity: A Numerical Study, J. Appl. Comput. Mech., 5(4) (2019) 791-803 DOI: 10.22055/JACM.2019.28147.1456

Waqas, H, Umar, F, Rabia, N, Sajjad, H, &Metib, A. (2021). Impact of MHD radiative flow of hybrid nanofluid over a rotating disk, Case Studies in Thermal Engineering 26 (2021) 101015, 1-13.

Waqas, H, Alqarni, M.S., Taseer, M.,& Muhammad A. K (2021), Numerical study for bioconvection transport of micropolar nanofluid over a thin needle with thermal and exponential space-based heat source, Case Studies in Thermal Engineering 26 (2021) 101158, 1-12.

Zhang, Y., Nazia, S, Muhammad, R., Hassan A, S, Ghazwani, M., & Malik, Y. (2021), Comparative analysis of Maxwell and Xue models for a hybrid nanofluid film flow on an inclined moving substrate, Case Studies in Thermal Engineering 28 (2021) 101598, 1-11.